# 3D Capturing of Fingerprints – On the way to a contactless certified sensor

D. Koller[1], L. Walchshäusl[1], G. Eggers[1], F. Neudel[1], U. Kursawe[1], P. Kühmstedt[2], M. Heinze[2], R. Ramm[2], C. Bräuer-Burchardt[2], G. Notni[2], R. Kafka[3], R. Neubert[3], H. Seibert[4], M. Castro-Neves[4], A. Nouak[4]

[1]TST Biometrics, Möhlstraße 39, 80912 Munich
dk@tst-biometrics.com;lw@tst-biometrics.com

[2]Abteilung Optische Systeme,
Fraunhofer Institut für Angewandte Optik und Feinmechanik IOF,
Albert-Einstein-Straße 7, 07745 Jena
peter.kuehmstedt@iof.fraunhofer.de;gunther.notni@iof.fraunhofer.de

[3]TRIOPTICS Berlin GmbH,
Schwarzschildstraße 12, 12489 Berlin
r.kafka@trioptics-berlin.com;r.neubert@trioptics-berlin.com

[4]Abteilung Identifikation und Biometrie,
Fraunhofer-Institut für Graphische Datenverarbeitung IGD,
Fraunhoferstraße 5, 64283 Darmstadt
alexander.nouak@igd.fraunhofer.de

**Abstract:** The purpose of this paper is to describe the development and performance tests of a contact-free fingerprint sensor, TrueFinger3D (TF3D). This contactless fingerprint sensor is designed to be perfectly interoperable with fingerprint image data captured with contact-based sensors or ink pads. This is achieved by acquiring a 3D dataset of the fingertip together with the image of the papillary lines. Based on the 3D data, the papillary lines image can be processed to compensate perspective foreshortening or even emulate deformation effects caused with contact-based sensors. The 3D measurement mechanism and the image processing are described in detail. The resulting fingerprint images taken by the contactless sensor are then matched with images taken by regular contact-based fingerprint readers at different force levels. The comparison shows that the geometric distortion of our contactless sensor TF3D is comparable to that of contact-based sensors deployed under regular conditions. Our test also shows that contact-based sensors operated under irregular or strong force conditions suffer from a substantial performance degradation, not seen with the contactless sensor TF3D, which has perfect reproducibility. The results also indicate perfect interoperability of the TF3D with any contact-based data and should therefore entitle the sensor to a certification for governmental use.

## 1 Motivation

Contact-based fingerprint sensors are state of the art devices for biometric identification in the government environment (i.e. border control). These sensors generally offer a high image quality and, due to the similarity of the image acquisition process, are compatible to ink-scanned legacy background databases, which enables an on the fly comparison with delinquent databases [BSL06, ABD+04]. However, contact-based sensors suffer from a number of drawbacks:

- The fingertip deformation caused by pressing the finger to the sensor surface causes significant and undeterminable distortions in the resulting images thus decreasing the matching rate.
- Users have hygienic concerns, especially in frequent used public environments like border control.
- The sensor surface suffers from abrasion and contamination which results in maintenance and cleaning costs.

The paper at hand reports on a contactless fingerprint sensor, which addresses these downsides and retains the compatibility to ink-scanned legacy data at the same time. The paper is organized as follows: Section 2 describes the sensor's technology, including the general setup, the 3D phase mapping (2.1), 3D data generation (2.2) and the projection and rendering process (2.3). Section 3 then presents a first evaluation including a comparative study of minutiae error ranges with contact-based sensors.

## 2 Technology and System Components

Our scanner acquires both the 3D structure and the papillary lines of a finger in one capturing process by a CMOS RGB camera. The 3D structure is deduced by means of structured

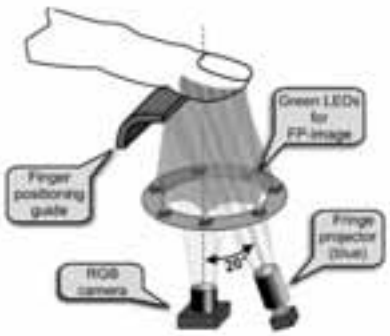


Figure 1: Scheme of the contactless fingerprint sensor.

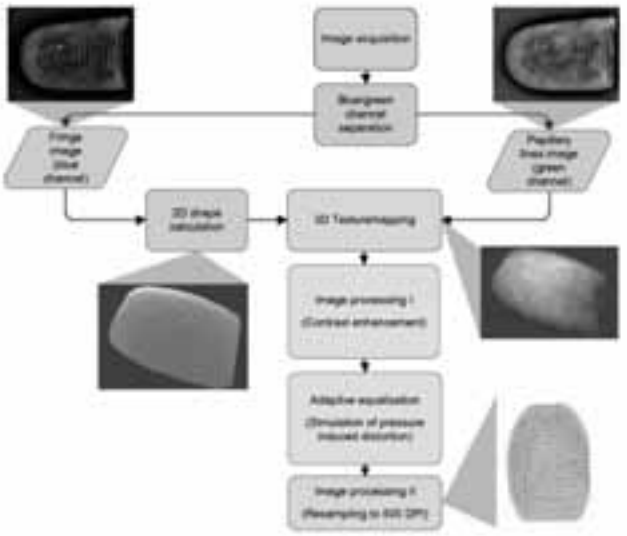

Figure 2: Overview of the capturing process of the scanner.

light [Gü02], which is projected onto the finger with a fringe projector. While the fringe projector operates at a blue wavelength, a green illumination is used to image the papillary lines. Thus, the 3D data and the papillary lines image can be separated by splitting the B and the G channel of the camera. Figure 1 shows the basic sensor setup.

### 2.1 Calculation of the Phase Map

The fringe projector uses a blue light source and projects a perfect sinusoidal pattern on the finger surface under grazing incidence (ca. 20°). The camera observes the fringe pattern deformed by the real shape of the finger in normal direction (i.e. perpendicular) to the measurement area. These images detected on the camera sensor are very similar to fringe patterns known from interferometry where well known interferometric analysis methods are being used to determine the desired phase image of the 3D finger shape [POE87, Sch90].The requirements for a short processing time of the entire finger print scanning demands to generate all necessary information in a single shot. Phase-stepping methods typically used in interferometry for higher accuracy consume too much measurement time and are not applicable here. The alternative methods are algorithms based on static fringe analysis, which determines the phase of each data point under the consideration that the interference pattern has parallel and equal-distant fringes in case on an error-free surface. Any deviation from that ideal fringe pattern can be seen as a deformation of the surface under test, i.e. the real shape of the illuminated finger. The nominal

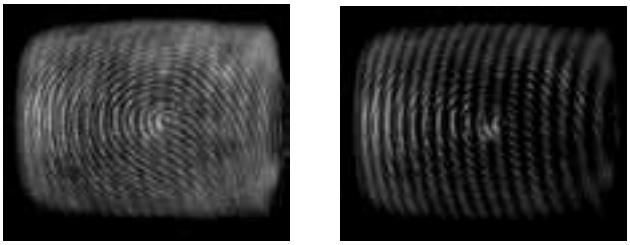

Figure 3: Sample green and blue channel image of the scanner. Please note the grey scale data of the camera channels has been matched to a green, resp. blue color scale.

fringe distance is used as a carrier frequency to separate the ideal pattern and the real deformation of the sample.

The special challenge for the phase calculation in the finger scanner application is the bad image quality compared with typical interferometric patterns. In Figure 3 it can be seen that the blue camera channel does not detect the fringe projection only: the fringes are disturbed by the papillary line patterns as well as from crosstalk between the camera's colour channels. The visibility of the fringe pattern is increased in a first analysis step by a special combination of the images from the blue and the green camera channel. The interruption of one of the fringes in the middle of the image is caused by an artificial structure in the pattern generator. We use that to detect the zero height reference needed to calculate the real 3D topography of the finger scanned (see section 2.2). Caused by the grazing projection and depending on the actual position of the free floating finger during the measurement, that fringe interruption is detected on varying camera pixels. But it has always the same fringe number in the optical system.

The phase image is calculated by a fringe tracking (FTR) method [KBVE93], with some adaption to the special fringe image types detected by the contactless finger print sensor. A 1D Fourier analysis is used in advance of the FTR to check the fringe direction and fringe density. Images not fullfilling the system-inherent limits (e.g. empty measurements, unusual shapes) are sorted out and the relating measurement must be repeated. The following FTR looks for the dark fringes (minima of the intensity) using a first order derivation across the main fringe direction [Sny80]. That results initially in a collection of single data points each representing a local intensity minimum.

The second step is the most important – and most difficult one in the phase determination: a highly specialized tracking algorithm connects the single points to fringes giving all points of the same fringe the same order number. Remaining data points with no connection to a fringe are deleted and lead to an area where no phase and finally no fingerprint can be reconstructed.

The last step of the phase determination is the calculation of the phase value at each image point. For that we simply use all numbered data points in one camera row (in case of mainly vertical fringes), set the phase difference between two succeeding orders to $2\pi$ and calculate the phase of all image points in-between by a spline interpolation. For a faster processing of the following topography reconstruction we set the zero order to the

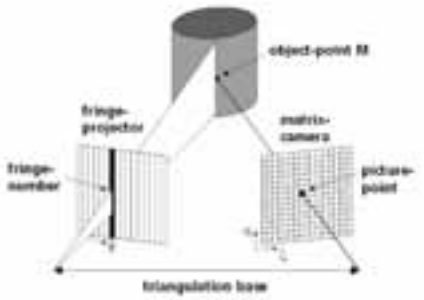


Figure 4: Measuring three dimensional points by triangulation.

interrupted fringe. The resulting phase map is more or less a tilted cylinder, deformed by the real finger and can now be converted to the 3D data needed to roll off the spatially detected fingerprint to a 2D map for comparison with certified references.

### 2.2 Calculation of the three dimensional finger shape

The technique used for 3D acquisition of the finger shape is based on fringe projection. In standard fringe projection a camera observes an object surface, which is illuminated by a projector with a sequence of crossed gray code- and sinus-patterns. Every point of the object surface is encoded in a defined according to the projected sequence. This coding is presented by the so-called phase map, which is generated from the intensity images of the camera as described in section 2.1. In the phase map each camera pixel is assigned with two-phase values. The phase map already includes the depth information of the surface. To calculate a proper three dimensional point cloud out of the phase map, the knowledge of the system parameters is necessary. These system parameters contain a range of optical and geometrical specifications of the camera and the projector system, which are determined in a preliminary processed calibration. Determination of the point coordinates in the calibrated system is obtained by triangulation which is illustrated in figure 4.

The standard fringe projection technique was modified for the 3D acquisition of the finger. Due to the simple and always similar shape of fingers the illuminated sequence is reduced to one sinus-pattern, which is sufficient for encoding the object surface points. Hence the projector gets very compact by integrating this sinus-pattern as a transparency directly into the optical lens system. The whole projector device consists of a blue LED, a condenser lens, the slide with the sinus-pattern and a lens. The pattern with 10 periods per millimetre gets displayed with 10-times magnification and a contrast of more than 90% on the finger. The pattern projected on the finger is observed by the camera at an angle of 20° according to the projector. The camera lens allows to measure the finger in a volume of 21 x 17 x 5 $mm^3$ with a lateral resolution of 25 $\mu m$. The fringe pattern is simultaneously measured with the fingerprint by a single shot of the camera. After that the phase map is

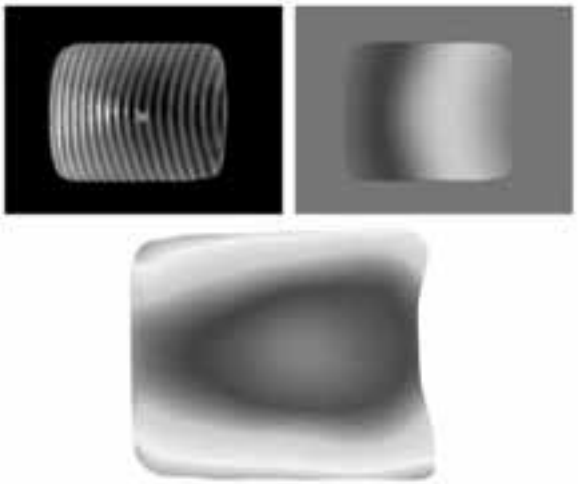

Figure 5: Point cloud of a fingertip (upper left: blue channel of the camera chip; upper right: phase map; lower: colour-coded point cloud).

calculated using Fourier transform of the data from the blue channel of the camera chip. In difference to standard fringe projection one period of the sinus pattern is labelled by a structure defining the absolute fringe number. The coordinates of the points are calculated by triangulation from the phase map and the system calibration parameters.

The aim of the calibration process is to obtain geometrical and optical specifications of one fixed projector/camera system, including all aberrations in the manufactured items. Standard calibration methods had to be modified because only one sinus-pattern was used. A simple procedure using algorithms from photogrammetry was developed. A plane surface with equidistant markings is used as calibration object. This object is measured with the fixed camera/projector system in three defined positions. By knowledge of the positions of the markings and the phase map it is possible to compute the necessary system parameters.

For the measurement of the three-dimensional fingers a calibrated system and the phase map of the finger is necessary. The resulting point cloud contains XYZ-coordinates sorted by the sensor element indices of the camera chip. The sorting is very important for the correspondence between the point cloud and the fingerprint map. The steps for acquiring a three dimensional point cloud are illustrated by Figure 5.

### 2.3 Projection and rendering of fingerprint images

The 3D finger reconstruction dataset acquired with the proposed sensor system consists in a two-dimensional field of measured 3D surface points and a texture depicting the finger surface. The texture image corresponds directly to the camera image produced by the optical system of the camera device including the aberration of the lens system. The

camera system has been calibrated in a preparatory step and the corresponding intrinsic and extrinsic parameters of the projection and camera system have been considered for the reconstruction process, e.g. the measured surface point coordinates are metrically correct within the accuracy limits of the sensor.

Interoperability of sensor devices is very important, e.g. the images shall be suitable for existing minutiae extraction algorithms that were designed to work with fingerprint images acquired with contact-based systems with capacitive sensors or FTIR sensors. A comparison of fingerprint images usually relies on the relative location and orientation of features, such as ridge endings, bifurcations islands, core points or deltas.

As the images produced by contact-based devices depict planar finger surfaces all measurements such as minutiae positions and orientations are determined within two-dimensional images.

The perspective projection of the fingerprint introduced in the camera based acquisition yields distortions by means of decreased distances between feature points depending on the distance of the observed surface portion. Regarding the shape of a fingertip we can clearly observe that the density of ridges increases from the image centre towards the image border. An ideal solution for this problem would require a projection method which projects the curved finger surface into a plane while preserving both, lengths and angles.

A similar problem is well known in the area of map projection, e.g. to create world maps. From a theoretical point of view the situation is quite clear: All map projection methods introduce some amount of distortion, a map projection might preserve distances (equidistant projection) or preserve shapes (conformal projection). Many projection methods have been introduced which realize an application specific optimum to preserve some properties of the sphere-like body at the expense of other properties [Sny93].

For our application there are two suitable ways: Use of a map projection providing a reasonable accuracy or the use of a nonparametric unwrapping to flatten the curved surface.

### 2.3.1 Map projection

The map projection approach requires some shape model to perform the projective transform of spherical or cylindrical coordinates into a plane. The Winkel-Tripel projection has been shown as a projection minimizing both errors [GI07]. For testing of the map projection approach two shape models have been used to approximate the finger shape: A combination of a quarter of a sphere and a cylinder, and an ellipsoid. The Winkel-Tripel projection formulas have been adapted by adding a constant scale factor on one axis in order to fit the cylinder radius. To perform mapping of an ellipsoid surface, the aspect of the ellipsoid radii has been used additionally to obtain reasonable scaled results.

### 2.3.2 Nonparametric unwrapping

The nonparametric unwrap approach [CPDSJ06] tries to preserve the distances between surface points, e.g. curves are stretched such that the distance between two points remains in the image plane. All points are shifted with respect to their neighbouring points. As

this approach considers a cylindrical shape model for the finger and propagates position changes from the centreline to the outer parts of the image, the dataset may be properly aligned using a least squares cylinder-fitting method in order to obtain proper results. A related approach [WHL10] uses elastic tube fit realized by fitting of many circles instead. Within the current work the approach mentioned at the beginning of this section has been modified in order to avoid a resampling of the surface, e.g. only existing surface points have been shifted to achieve a flattened surface.

### 2.3.3 Rendering of fingerprint images

After projection, which maps the 3D points to a single plane in three-dimensional space the final fingerprint image can be generated by surface-rendering based on the implicit triangulation of the measured surface points. Direct texture mapping without shading is applied to preserve the grey scales of the texture image. Results of the discussed projection approaches are depicted in Figure 6. Before rendering the texture image may be pre-processed in order to remove inhomogeneous illumination and to approximate the appearance of FTIR images.

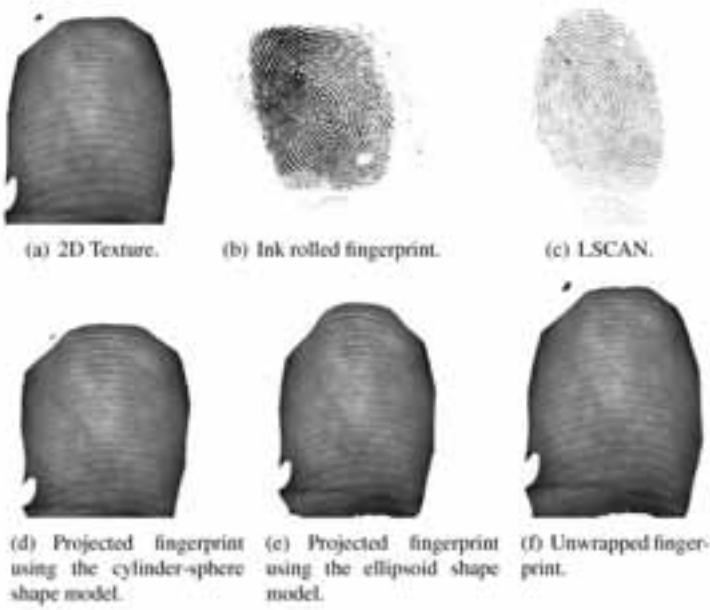

(a) 2D Texture. (b) Ink rolled fingerprint. (c) LSCAN.

(d) Projected fingerprint using the cylinder-sphere shape model. (e) Projected fingerprint using the ellipsoid shape model. (f) Unwrapped fingerprint.

Figure 6: Different projection methods in comparison.

The projection approaches discussed above provide results which appear satisfactory, judged on a visual basis. The numerical evaluation of the projection results based on original fingers is not feasible if the real shape is not known, the errors can only be evaluated for well-known reference objects. Due to the principal problem that an ideal projection does

not exist and that the discussed methods involve approximations of shape models or physical constraints the numerical evaluation is omitted here.

As the real problem is the interoperability with contact-based systems, the evaluation of the projection results based on minutiae locations compared to minutiae locations measured with contact-based sensors might provide most valuable results.

For the following evaluation the datasets have been registered using an ellipsoid fitting to align the principal axes of the ellipsoid to the coordinate axes. After transformation of all points according to the registration an optimized nonparametric unwrapping approach has been used in order to reduce the computational efforts.

# 3 Evaluation

An important criterion for contactless fingerprint sensors is the geometric compatibility of captured fingerprint images with images from contact-based sensors, to ensure biometric matching interoperability. The next sections describe our annotation and comparison approach to approximate and quantify this geometric compatibility as well as deduced results in respect of contact-based and contactless interoperability [CCK10] .

## 3.1 Annotation and comparison approach

We propose a semi-autonomous correspondence annotation scheme to measure the amount of geometric compatibility between fingerprint images. First, corresponding salient reference points (i.e. minutiae locations) are labelled in two fingerprint images by a human operator using a dedicated annotation software (see Figure 7). The human operator is assisted by an automatic generated first guess of corresponding points. Important for a sufficient geometry approximation is a homogenous and complete coverage of the fingerprint images. In the next step the resulting point clouds of the fingerprint images are aligned such that the distances of corresponding points are minized. Currently, we align the point clouds at the mean and determine a rotation angle between the two point clouds, which ensures minimal average point-to-point distances. Other alignment strategies like spring models are thinkable. The maximum distance between corresponding points and the average distance of all corresponding points are useful metrics and are therefore utilized to approximate for the geometric compatibility of the annotated fingerprint images.

## 3.2 Data acquisition and results

Fingerprint images were captured of several fingers from a contact-based scanner (we used a Crossmatch LScan device but any other contact-based sensor excluding swipe sensors would result in comparable distortions) and our contactless scanner (TF3D). For each

Figure 7: (a) Labelling software to annotate corresponding points in TF3D finger images (left fingerprint image) and contact-based scanner images (right fingerprint image). (b) Resulting corresponding points.

finger 15 captures were taken: 5 captures with the contact-based sensor with 7 Newton contact pressure (best case data set abbreviated with KBS7N), 5 captures with the contact-based sensor with 30 Newton contact pressure (worst case data set with lateral displacements while capture abbreviated with KBS30N) and 5 captures with the contactless sensor (abbreviated with TF3D). See also Figure 8 for sample captures. Between each capture the finger was removed and replaced to ensure a natural variation between the captures.

Figure 8: Samples of fingerprint data from a forefinger used in the evaluation. The first row contains LScan samples with 7N contact pressure. The second row contains LScan samples with 30N contact pressure at simultaneous lateral distortions (left, right, up, down, rotational). The third row contains contactless fingerprint captures.

After data acquisition correspondent point clouds were determined with the annotation tool described in Section 3.1 between fingerprint images from data sets KBS7N vs. KBS7N

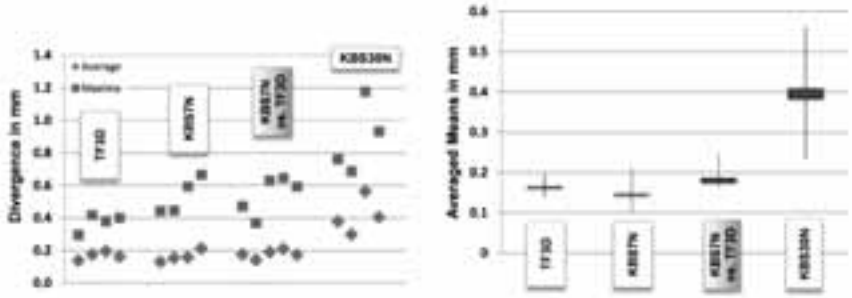


Figure 9: Maximum (dark squared) and averaged (light diamonds) divergences in millimetre show a comparable interoperability (column 3) and intraoperability (column 1, 2, and 4).

(abbr. with KBS7N), from data sets KBS30N vs. KBS30N (abbr. with KBS30N), from data sets TF3D vs. TF3D (abbr. with TF3D) and between images from data sets TF3D vs. KBS7N. Figure 9(a) shows the typical results for one finger and Figure 9(b) the averaged results for all captured fingers. It can be seen, that the averaged geometrical distortions are around 0.2 mm for the KBS7N, TF3D and KBS7N vs. TF3D data group. Average geometrical distortion values of the KBS30N data set are twice as high and the maximum distortion values are significant higher.

To estimate the distortion accuracy of the manually labelled fingerprints we calculated the distances of individually annotated identical fingerprints and got a maximum distance of 0.15 and an average distance of 0.05 mm. These values have to be added to the overall variance.

Thus, the evaluation results show, that the geometrical distortion of our contactless sensor TF3D is comparable to the geometrical distortions of contact-based sensors and even lower in the case that contact-based sensors are operated under worst case conditions. The significant amount of distortion observed with contact-based scanners conforms to measurements presented in [MD04].

## 4 Summary

We have presented the technical concept of a contactless fingerprint scanner equipped with a 3D fingertip scanning technology allowing a de-convolution of the curved fingertip surface into a 2D fingertip image. Comparative measurements with a contact-based scanner show a comparable uncertainty and error range, which indicates perfect interoperability of the TF3D sensor. This TF3D contact-free fingerprint scanner is therefore suitable for governmental use and should pass all required certification tests. An adaptation of the respective Technical Guideline TR03104 ([BSIa, BSIb]) to include also contactless fingertip sensors is therefore under discussion with the German Federal Office for Information Security (BSI). This conjoint research and development project has been funded by the ZIM initiative of the Federal Ministry of Technology and Economics (BMWi) on the basis of the decision by the German Bundestag.

## References


[ABD+04] Michael Arnold, Christoph Busch, Martin Drahanský, Heinrich Ihmor, Tom Reinefeld, and Alexander Zwiesele. BioFinger - Evaluierung biometrischer Systeme (Fingerabdrucktechnologien). Technical report, 2004.

[BSIa] BSI - Bundesamt für Sicherheit in der Informationstechnik. BSI TR-03104 – Technische Richtlinie zur Produktionsdatenerfassung, -qualitätsprüfung und -übermittlung für Pässe, Version 2.1.5.

[BSIb] BSI - Bundesamt für Sicherheit in der Informationstechnik. BSI TR-03104 Annex 2 (QS-Finger) – Technische Richtlinie zur Produktionsdatenerfassung,-qualitätsprüfung und -übermittlung für Pässe, Version 2.1.5 – Qualitätsanforderungen bei der Erfassung und Übertragung der Fingerabdrücke als biometrische Merkmale für elektronische Pässe.

[BSL06] University of Bologna Biometric System Laboratory. FVC2006: the Fourth International Fingerprint Verification Competition, Biometric System Laboratory, 2006.

[CCK10] Heeseung Choi, Kyoungtaek Choi, and Jaihie Kim. Mosaicing Touchless and Mirror-Reflected Fingerprint Images. *Information Forensics and Security, IEEE Transactions on*, 5(1):52 –61, march 2010.

[CPDSJ06] Yi Chen, G. Parziale, E. Diaz-Santana, and A.K. Jain. 3D Touchless Fingerprints: Compatibility with Legacy Rolled Images. In *Biometric Consortium Conference, 2006 Biometrics Symposium: Special Session on Research at the*, pages 1–6, 2006.

[GI07] David M. Goldberg and J. Richard Gott III. Flexion and Skewness in Map Projections of the Earth. *Cartographica*, 42(4):297–318, 2007.

[Gü02] Jens Gühring. *3D-Erfassung und Objektrekonstruktion mittels Streifenprojektion*. PhD thesis, Universität Stuttgart, Holzgartenstr. 16, 70174 Stuttgart, 2002.

[KBVE93] Ricarda Kafka, Thomas Blümel, Andreas Vogel, and Karl-Edmund Elßner. Static Fringe Evaluation of Technical Interferograms. In *Physical Research*, volume 19, pages 88–90. Akademie-Verlag Berlin, 1993.

[MD04] S. Mil'shtein and U. Doshi. Scanning the pressure-induced distortion of fingerprints. *Scanning*, 26(6):270–272, 2004.

[POE87] P.Hariharan, B.F. Oreb, and T. Eiju. Digital Phase-Shifting Interferometry: A Simple Error-Compemsating Phase Calculation Algorithm. *Applied Optics*, 26(13):2504––2506, 1987.

[Sch90] Johannes Schwider. Advanced Evaluation Techniques in Interferometry. In E. Wilf, editor, *progress in optics*, volume XXVIII, pages 271–359. Ed. Elsevier Science Publishers, 1990.

[Sny80] J.J. Snyder. Algorithm for fast digital analysis of interference fringes. *Applied Optics*, 19(8):1223—1225, 1980.

[Sny93] J. P Snyder. *Flattening the Earth-Two thousand years of map projections*. The University of Chicago Press Ltd, London, 1993.

[WHL10] Y. Wang, L. G. Hassebrook, and D. Lau. Data Acquisition and Processing of 3-D Fingerprints. *IEEE Transactions on Information Forensics and Security*, 2010.